Shedding light on topological superconductors

K. H. A. Villegas,[1] V. M. Kovalev,[2,3] F. V. Kusmartsev,[4,5] and I. G. Savenko[1,6]

[1] *Center for Theoretical Physics of Complex Systems, Institute for Basic Science (IBS), Daejeon 34126, Korea*
[2] *A.V. Rzhanov Institute of Semiconductor Physics, Siberian Branch of Russian Academy of Sciences, Novosibirsk 630090, Russia*
[3] *Department of Applied and Theoretical Physics, Novosibirsk State Technical University, Novosibirsk 630073, Russia*
[4] *Department of Physics, Loughborough University, Loughborough LE11 3TU, United Kingdom*
[5] *Micro/Nano Fabrication Laboratory Microsystem and THz Research Center, Chengdu, Sichuan, China*
[6] *Basic Science Program, Korea University of Science and Technology (UST), Daejeon 34113, Korea*

(Received 27 April 2018; revised manuscript received 13 July 2018; published 7 August 2018)

We propose an effective optical approach to monitor superconductors in a two-layer superconductor-normal metal structure. Effectively, such a hybrid system represents a resonator, where electrons are strongly coupled with light. We show that the interaction of light with the superconductor is strongly boosted in the presence of the neighboring metal and, as a result, the electromagnetic power absorption of the system is dramatically enhanced. It manifests itself in a giant Fano-type resonance which can uniquely characterize the elementary excitations of the system. Our approach is especially promising for topological superconductors, where Majorana fermions could be revealed and controlled by light.

DOI: 10.1103/PhysRevB.98.064502

I. INTRODUCTION

Superconductivity is conventionally considered to be a material property difficult to characterize with light, due to weak light-matter interaction in superconducting condensates. To test whether materials are superconductors, electric (resistivity-based) and magnetic (Meissner effect-based) techniques are routinely used. However, optics would be very helpful if we want to monitor hybrids of such fascinating classes of materials as topological insulators (TI) [1–5] and Weyl semimetals (WM) [6–13]. In this framework, superconductors should be considered as candidates to reveal new topological properties, thus fostering a revisit of existing experimental techniques.

Topological superconductors behaving metallic on the surface and superconducting in the bulk naturally combine the properties of both metal and superconductor, which is the key problem for their discovery. On one hand, electrical conductivity measurements used to study conventional superconductors have proved to be challenging due to a mutual influence of the free electrons associated with the metallic surface and the Cooper pairs of the superconducting bulk. On the other hand, diamagnetic Meissner magnetization measurements require a minimal volume, which is an issue for surface topological superconductivity.

In this paper, we propose an optical approach to monitor the behavior of superconductors. As an important ingredient, it requires coupling of the superconductor to a metallic layer with plasmonic gapless excitations. Their hybridization with flat bands and superconducting excitations leads to a giant light absorption due to a high density of states. As a result, a film of topological material deposited on the thin metallic layer will have hybrid elementary excitations. The significant result that we demonstrate below is that these excitations are highly optically active; they display strong resonances in optical absorption measurements, thereby characterizing the material under study.

Various hybrid normal-metal–superconductor or semiconductor-superconductor systems, in which a two-dimensional electron gas (2DEG) is in contact with Cooper pairs, have been broadly considered in literature. Examples of the widespread implementation of such hybrid systems include a Josephson junction or a Josephson tunnel junction [14] aimed at cooling (as a heat sink), observation of Majorana fermions [15,16] and zero modes [17,18], and an enhancement of the degree of photon pair entanglement [19]. Furthermore, recent studies show that there are advantages in using optical scattering and surface plasmons especially in the context of plasmon-based refractive index sensing [20]. It was shown that graphene-based plasmonic sensors have higher surface sensitivity than conventional ones and, further, the light scattering of plasmons can be controlled by a dc current and external bias voltage [21]. Moreover, the method developed in these papers has been demonstrated to be effective to study nonlocal response to detect the presence of adatoms and impurities [22–24].

Recently, it was shown that hybrid systems also allow new mechanisms of superconductivity itself using interaction with excitons [25] or exciton polaritons [26,27] in semiconductor structures, where the latter can serve as an auxiliary to increase T_c. From an application-oriented perspective, semiconductor-based hybrid structures can be employed in such devices as tunnel diodes [28] and optoelectronic circuits for high-bandwidth information processing [29,30]. Furthermore, the most recent advances in molecular beam epitaxial heterostructure growth techniques suggest a route to create high-quality hybrid structures [31].

We show here that a metallic layer located in the vicinity of a superconductor can dramatically enhance light-superconductor coupling, such that the superconducting properties can ultimately be well characterized by the absorption spectrum of the hybrid system. Specifically, we demonstrate that the system reveals a giant hybrid Fano resonance [32,33], which arises in both normal and superconducting hybrid subsystems due to their mutual influence. The shape and positions of the peaks (and the dip) of the Fano resonance may uniquely characterize both the superconducting and metallic subsystems, especially the value of the superconducting gap and therefore the order parameter, its symmetry, and critical temperature. Thus, our findings open a prospective method, being optical and noninvasive, for the characterization and testing of materials for superconductivity.

II. SYSTEM SCHEMATIC AND HYBRID EIGENMODES

Let us consider a system with two parallel layers of a normal metal and a superconductor, as illustrated in Fig. 1(a). The two layers are assumed to be sufficiently well separated (10^{-6}–10^{-5} cm) so that tunneling and proximity effects can be safely disregarded. The electrons in the normal metal interact via Coulomb interaction, which has the Fourier image given by $v_k = 2\pi e^2/k$, where $\mathbf{k}$ is in-plane momentum (lying in the xy plane). The electrons between the two layers are also Coulomb coupled, and the Fourier image of the interlayer interaction reads as $u_k = 2\pi e^2 \exp(-ak)/k$, where a is the separation between the layers. The electromagnetic wave is polarized along the x axis, $\mathbf{E}(\mathbf{r},t) = \hat{\mathbf{x}} E_0 e^{-i(k_\perp z + \mathbf{k}_\parallel \cdot \mathbf{r} + \omega t)}$ where $\mathbf{k}_\parallel$, ω, and $\mathbf{r}$ are the in-plane wave vector of the field, frequency, and coordinate, respectively.

Using the polarization functions of the 2DEG and superconductor [see Appendix A, Eqs. (A2) and (A3) and [34,35]], we solve the eigenvalue problem and find two branches of dispersion of the hybrid modes (assuming a topologically trivial case of constant Δ):

$$\omega_\pm^2(k) = 2\Delta^2 + e^2 k\left(\frac{p_{NF}^2}{m_N} + \frac{p_{SF}^2}{m_S}\right) \pm \frac{1}{2}\sqrt{\xi_- \xi_+ - 4\beta_k^2}, \quad \text{where}$$

$$\xi_\pm = \left[\left(2\Delta \pm e p_{NF}\sqrt{\frac{k}{m_N}}\right)^2 + \frac{e^2}{m_S} p_{SF}^2 k\right],$$

$$\beta_k^2 = \frac{e^4 p_{NF}^2 p_{SF}^2}{m_N m_S} k^2 (1 - e^{-2ka}). \tag{1}$$

Here, 2Δ is the superconducting gap, $e > 0$ is elementary charge, p_{SF} and p_{NF} are the Fermi momenta in the superconductor and normal layer, respectively, and m_S and m_N are effective electron masses. Figure 1(b) shows the hybrid modes for $m_N = m_S$ (with bare modes presented for comparison).

III. ELECTROMAGNETIC POWER ABSORPTION BY 2DEG

Further, assuming a linear response of the system, the Fourier component of the current in the 2DEG layer can be written as $j_{k_\parallel,\omega}$. Both the wave vector and frequency of current density have specific values fixed by the external electromagnetic field; the following formula can therefore be used to compute the time-averaged power absorbed by the hybrid system as a function of frequency ω:

$$\mathcal{P}(\omega) = \frac{1}{2}\left\langle \mathrm{Re} \int d^2 r\, \mathbf{J}(\mathbf{r},t) \cdot \mathbf{E}^*(\mathbf{r},t) \right\rangle,$$

where the integration is over the plane of the normal metal sample and $\langle \ldots \rangle$ denotes time averaging. Normalizing $\mathcal{P}(\omega)$ by $\int d^2 r = l^2$ and utilizing the continuity equation $k j_{k,\omega} = -e\omega \delta n_{k,\omega}$, where $\delta n_{k,\omega}$ describes fluctuations of the electron density in the 2DEG (see the explicit formula in Appendix A 1), we obtain the specific power absorption coefficient (hereafter simply referred to as *power absorption*):

$$P_1(\omega) = \frac{1}{2}\frac{e\omega}{k} |\mathrm{Re}(\delta n_{k,\omega})| E_0. \tag{2}$$

This formula accounts for the electron-electron and electron-Cooper pair interaction as well as the coupling of both the

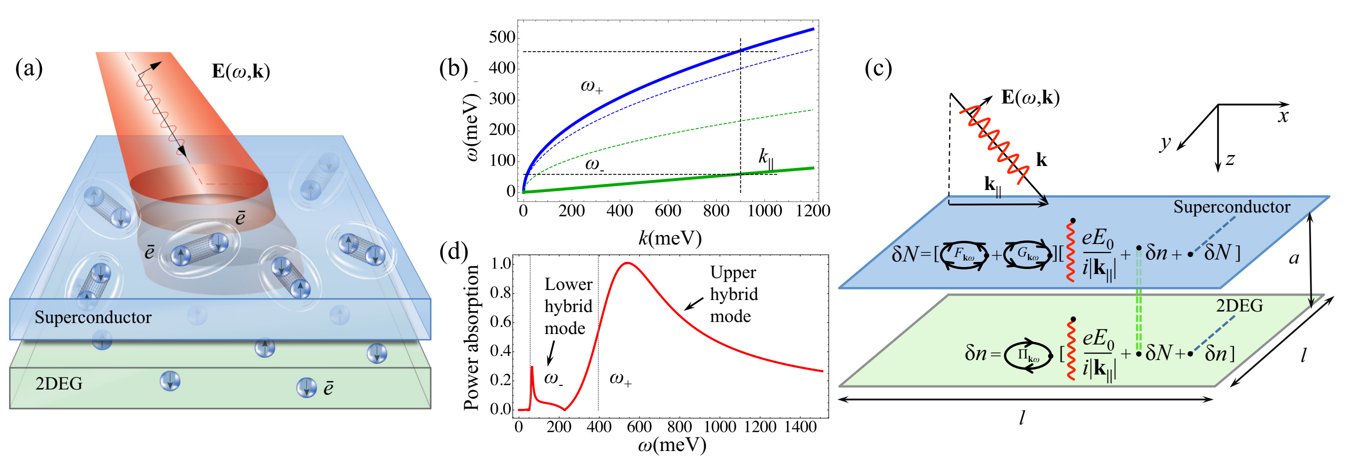

FIG. 1. System schematic. (a) Hybrid normal-metal–superconductor structure exposed to an electromagnetic field of incident light. (b) Dispersions of hybrid eigenmodes of the system: ω as a function of k for $m_N = m_S = 1$ (green and blue solid curves). The dashed curves of the corresponding colors show the individual modes of each layer when the interlayer interaction is switched off. (c) Schematic of in-layer, interlayer, and light-matter interactions in the system manifesting itself in fluctuations of electron and Cooper pair densities, δn and δN, and polarization operators $F_{\mathbf{k}\omega}$, $G_{\mathbf{k}\omega}$, and $\Pi_{\mathbf{k}\omega}$. (d) Spectrum of electromagnetic power absorption demonstrating the Fano resonance profile.

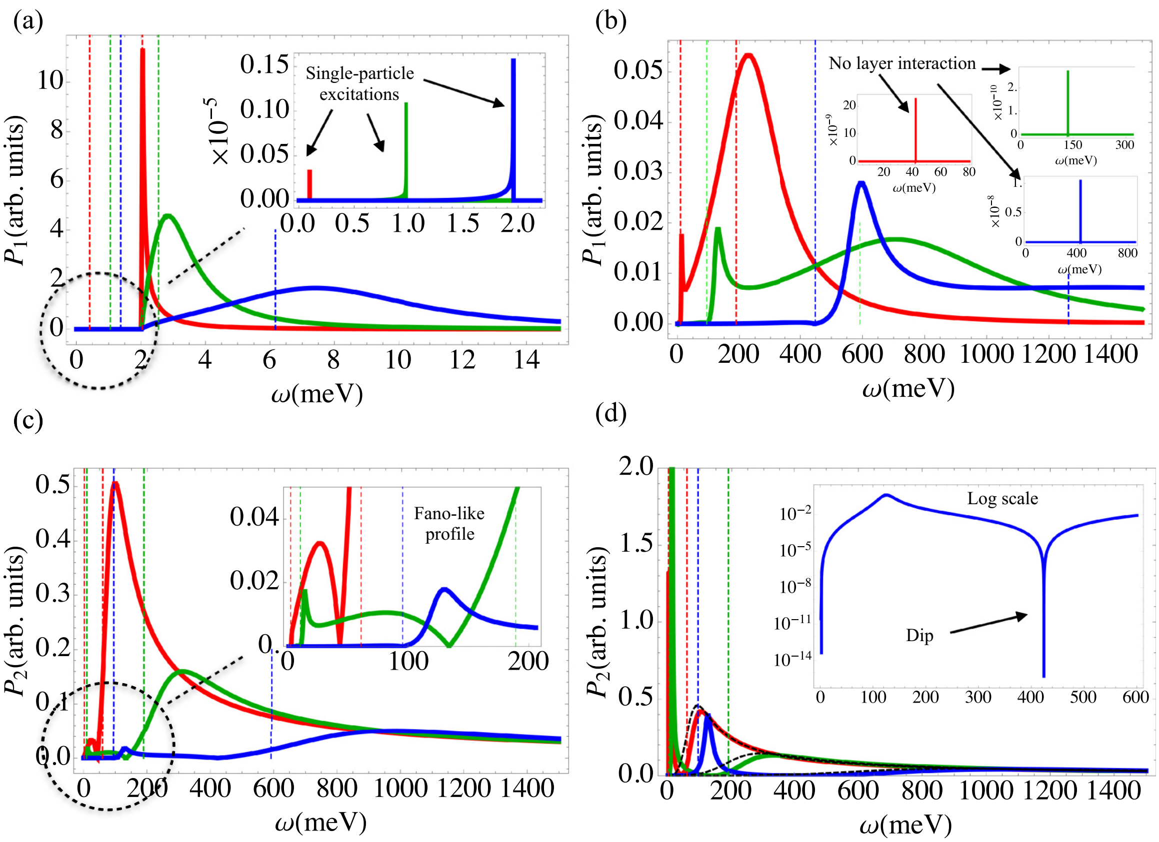

FIG. 2. Spectra. Power absorption monitored in 2DEG [(a), (b)] and superconductor [(c), (d)] as a function of ω for $\Delta = 1.0$ meV. Vertical dashed lines stand for the corresponding locations of the hybrid modes [within Eq. (1)]. (a) $k = 1.0 \times 10^{-3}$ (red curve), 1.0×10^{-2} (green curve), and 1.0×10^{-1} meV (blue curve). Inset shows the range $0 \leqslant \omega < 2\Delta$, contributions to $P_1(\omega)$ due to single-particle excitations. To render these contributions visible, larger k's were used: $k = 5.0 \times 10^1$ (red curve), 5.0×10^2 (green curve), and 1.0×10^3 (blue curve). (b) $k = 1.0 \times 10^1$ (red curve), 1.0×10^2 (green curve), and 1.0×10^3 meV (blue curve). Inset shows the case with no interlayer interaction. (c) Both layers are exposed to the EMF. Inset: zoom-in for small ω's showing peaks caused by the lower hybrid modes. (d) No external field on the normal layer. Inset shows the log plot of the corresponding blue curve, manifesting the two peaks and the dip of the Fano resonance. In (c) and (d), $k = 1.0 \times 10^1$ (red curves), 1.0×10^2 (green curves), 1.0×10^3 meV (blue curves). Dashed black curves in (d) show the case when interlayer coupling is turned off.

2DEG and superconductor to light [see the schematic description of corresponding processes in Fig. 1(c)].

The resulting power absorption by the hybrid system is presented in Fig. 1(d), where due to the interplay of different interaction mechanisms, we observe a Fano resonance. Let us consider the spectrum in detail. Figure 2 shows the power absorption as a function of ω for different wave vectors k when the hybrid structure is exposed to the EMF. In Fig. 2(a), the lower hybrid modes are below 2Δ and their contribution to the power absorption is suppressed, as can be seen by the lack of visible peaks in the vicinity of the three leftmost dashed lines. The inset shows the contribution of the single-particle excitations. As can be seen, this contribution is negligible compared to the contribution of the hybrid modes (three peaks of the main plot). The locations of the peaks at higher frequencies nearly coincide with the corresponding dashed lines, showing that these peaks are primarily due to the upper hybrid modes. As k increases, we observe a broadening (from red to blue curves).

Figure 2(b) shows the power absorption for larger values of k. The lower hybrid modes now have significant contributions, as can be seen by the existence of three sharp peaks, since they are now located above the gap. For comparison, the inset shows the power absorption when the interlayer coupling is switched off. It shows a disappearance of the contribution from the upper hybrid modes primarily due to the superconductor. Comparison of the lower-mode contributions shows that the presence of the superconductor enhances the power absorption of the hybrid system by six to eight orders of magnitude. Otherwise, the presence of the external EMF and the 2DEG does not dramatically influence the superconductor itself, and thus may serve as an auxiliary to monitor its behavior.

IV. ELECTROMAGNETIC POWER ABSORPTION BY SUPERCONDUCTOR

We can follow a similar procedure to calculate Cooper pair current in the superconductor. The power absorption then reads as (see derivations in Appendix A 2)

$$P_2(\omega) = \frac{1}{2}\frac{2e\omega}{k}|\mathrm{Re}(\delta N_{k\omega})|E_0, \tag{3}$$

where $\delta N_{k\omega}$ are Cooper pair density fluctuations in the superconducting layer.

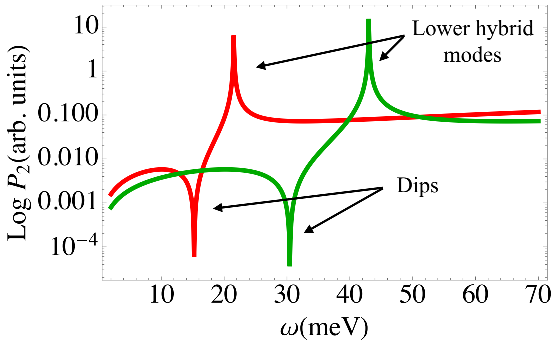

FIG. 3. Spectrum in topologically nontrivial case. Power absorption (in log scale) monitored in superconductor as a function of ω at $k = 0.5 \times 10^{-1}$ meV (red) and $k = 1.0 \times 10^{-1}$ meV (green).

Figure 2(c) shows the power absorption spectrum for different k's when both the 2DEG and superconductor are exposed to EMF. We observe a celebrated Fano resonance structure of the spectrum (inset). Figure 2(d) shows the power absorption when the external EMF at the normal layer is turned off. We immediately note that the contribution of the upper hybrid modes to the absorption spectrum is not significantly affected by switching off the field at the normal layer, as can be seen by comparing Figs. 2(c) and 2(d). This behavior is quite expected. Surprisingly, though, the contribution of the lower hybrid modes shows significant increase compared to the situation when the external field in the normal layer is switched on. Thus, we realize that the electronic layer must be very sensitive to the behavior of the superconductor, whereas the latter does not pay much attention to either the 2DEG or the light field. Indeed, switching off the interlayer interaction removes the contribution of the lower modes, as expected [dashed black curves in Fig. 2(d)]. We see that the second peak, which is mostly determined by the superconductor, remains nearly the same. Inset shows that in log scale, we observe both the two peaks of the Fano-type resonance and the dip.

Now, let us consider the nontrivial topology (p-wave pairing). Then, the superconducting gap reads as $\Delta_{\mathbf{k}} = f(k)(k_x - ik_y) = f(k)ke^{-i\phi}$, where ϕ is the polar angle measured with respect to the k_x axis in k space and the function $f(k)$ depends on the concrete p-wave superconductor; it should be finite for all $k \in [0,\infty)$ and vanish as $k \to \infty$ (see all the calculations in Appendices B 3 and B 4). The dependence of the superconducting gap $2\Delta_{\mathbf{k}}$ on $\mathbf{k}$ makes calculations more tricky but leads to qualitatively similar results. Figure 3 shows the resulting P_2 [compare with Fig. 2(c), green curve]. It should be noted that here the Fano-type dip is shifted to the frequency range below the first (lower hybrid mode) peak.

V. DISCUSSION

Herewith, we suggest a way to prepare samples of various hybrid-structured materials to test them for being superconductors via optics. That is, the proposed effect of the giant hybrid Fano resonance can be observed by measuring the optical response of two-layer metal-superconductor systems composed of, for example, superconducting niobium film deposited on a thin metallic layer of copper, gold, silver, or tin. The proposed effect can be used to design various sensors and diagnostics of superconducting magnets with light.

It should be noted that strong inhomogeneity and impurities can significantly modify the conductivity and plasmonic properties of 2DEG and may even produce a level splitting with the plasmon mode, resulting in two plasmon branches. It is similar to the effect of adatoms in graphene (for a detail, see [22]). The impurities are, in general, expected to modify the electromagnetic response and plasmon excitations and may generate new phenomena. Similar effects were investigated in graphene [20,22,23]. The microscopic treatment developed in these papers has shown that graphene plasmonic spectra are highly sensitive to impurities, that highlighted their strong potential for sensing purposes. Although these effects are interesting and might be important to investigate in hybrid systems, we leave it for the future works.

Our results also open the possibility of an alternative optical method of detecting Majorana fermions in topological superconductors. As shown in Ref. [36], Majorana fermions may induce resonant Andreev reflection from the lead to the grounded superconductor. Indeed, such tunneling zero-bias peaks have been observed experimentally in superconducting nanowires and interpreted as signatures of Majorana fermions [15,36–40]. However, due to the elusiveness of the Majorana fermions and the lack of control to confirm these experimental findings, an alternative method is still utmost required.

In this paper we propose to study the light absorption into the zero-energy level associated with the Majorana fermions. To some extent, it is equivalent to the tunneling experiments. However, instead of tunneling, we propose to use light interaction and plasmons to excite the electrons from or to the zero mode, where a Majorana must be located. In [41], Chen *et al.* proposed a similar (to some extent) optical method for Majorana detection based on a hybrid quantum dot nanomechanical resonator. However, in that paper two types of pump and probe laser fields are required to excite and measure the complex hybrid system. In contrast to that technique, in our approach the key element is strong plasmon coupling which produces a giant hybrid resonance and that should provide a major advantage over the former approach.

Moreover, the recent discovery of high-temperature light-induced superconductivity in K_2C_{60} [42] has stimulated an activity in the scientific community to test materials with light. Thus, our finding of enhanced light coupling in metal-superconducting hybrids alongside the possibility of testing is expected to open a new direction in this activity since it creates many opportunities for discoveries of condensed states induced by light.

VI. CONCLUSIONS

We have studied the linear response of a hybrid two-dimensional electron-gas–superconductor system to an external electromagnetic field of light. Such systems have hybrid excitations that originate from gapless plasmons of the two-dimensional electron gas of the metallic layer and gapful Bogoliubov excitations of the bulk superconductor.

TABLE I. Summary of the power absorption results (in topologically trivial case). Symbols L and R stand for the left-hand-side and right-hand-side peaks, respectively. The variables $\omega_{\max}$, $P_{\max}$, and γ denote the central frequency, the maximum power absorption, and the width of each peak, respectively. The width is defined as full width at half-maximum $P_{\max}/2$.

			Wave vector k (meV)		
Current monitored in	Ext. **E** present in	Peak	1.0×10^2	1.0×10^3	5.0×10^3
2DEG	Both layers	L	$\omega_{\max} = 7.68$ $P_{\max} = 0.018$ $\gamma \lessapprox 10$	$\omega_{\max} = 130$ $P_{\max} = 0.019$ $\gamma \sim 50$	$\omega_{\max} = 594$ $P_{\max} = 0.028$ $\gamma \sim 100$
		R	$\omega_{\max} = 223$ $P_{\max} = 0.054$ $\gamma \sim 200$	$\omega_{\max} = 700$ $P_{\max} = 0.017$ $\gamma \sim 300$	$\omega_{\max} \sim 1500$ $P_{\max} \sim 0.007$ $\gamma \sim 500$
	2DEG only	L	$\omega_{\max} = 8.77$ $P_{\max} = 4.0$ $\gamma \lessapprox 10$	$\omega_{\max} = 123$ $P_{\max} = 0.45$ $\gamma \lessapprox 50$	$\omega_{\max} = 583$ $P_{\max} = 0.16$ $\gamma \lessapprox 100$
		R	$\omega_{\max} = 200$ $P_{\max} = 0.02$ $\gamma \sim 100$	$\omega_{\max} = 600$ $P_{\max} = 0.01$ $\gamma \sim 200$	too broad
			Wave vector k (meV)		
			1.0×10^1	1.0×10^2	1.0×10^3
Supercond.	Both layers	L	$\omega_{\max} = 19$ $P_{\max} = 0.037$ $\gamma \sim 30$	$\omega_{\max} = 10$ $P_{\max} = 0.023$ $\gamma \lessapprox 10$	$\omega_{\max} = 125$ $P_{\max} = 0.022$ $\gamma \sim 20$
		R	$\omega_{\max} = 96.9$ $P_{\max} = 0.51$ $\gamma \sim 100$	$\omega_{\max} = 309$ $P_{\max} = 0.16$ $\gamma \sim 200$	$\omega_{\max} = 1022$ $P_{\max} = 0.054$ $\gamma = 600$
	Supercond. only	L	$\omega_{\max} = 2$ $P_{\max} = 1.3$ $\gamma \lessapprox 10$	$\omega_{\max} = 10$ $P_{\max} > 2$ $\gamma \lessapprox 10$	$\omega_{\max} = 124$ $P_{\max} = 0.40$ $\gamma \sim 50$
		R	$\omega_{\max} = 101$ $P_{\max} = 0.42$ $\gamma \sim 100$	$\omega_{\max} = 305$ $P_{\max} = 0.14$ $\gamma \sim 200$	$\omega_{\max} = 1000$ $P_{\max} = 0.04$ $\gamma \sim 1000$

We have calculated these hybrid eigenmodes of the system and investigated the electromagnetic power absorption spectra (see Table I for the summary). We find that these excitations exhibit a very strong coupling with the electromagnetic radiation, and show that they display giant Fano resonances associated with a large light absorption. Such results therefore indicate a way to monitor the behavior of a superconductor exposed to light by measuring the spectrum of photoabsorption of the two-dimensional electron gas.

ACKNOWLEDGMENTS

We thank S. Flach for useful discussions, J. Rasmussen (RECON) for a critical reading of our manuscript, and E. Savenko for help with the figures. V.M.K. has been supported by the Russian Foundation for Basic Research (Project No. 16-02-00565). K.H.V. and I.G.S. acknowledge the support of the Institute for Basic Science in Korea (Project No. IBS-R024-D1).

APPENDIX A: GENERAL FORMALISM

Let us consider a system presented in Fig. 1(a) in the main text, in which an electromagnetic field (EMF) interacts with the hybrid superconductor–2DEG system. The polarization function of a (topologically trivial) superconductor at zero temperature can be presented in the form [34] [see also Fig. 1(c) in the main text]

$$P_{\mathbf{k}\omega} = \frac{1}{2}\sum_{\mathbf{p}} \frac{E_{\mathbf{p}}E_{\mathbf{p}+\mathbf{k}} - \xi_{\mathbf{p}}\xi_{\mathbf{p}+\mathbf{k}} - \Delta^2}{E_{\mathbf{p}}E_{\mathbf{p}+\mathbf{k}}}\left(\frac{1}{\omega + i\delta - E_{\mathbf{p}} - E_{\mathbf{p}+\mathbf{k}}} - \frac{1}{\omega + i\delta + E_{\mathbf{p}} + E_{\mathbf{p}+\mathbf{k}}}\right) = G_{\mathbf{k}\omega} + F_{\mathbf{k}\omega}, \tag{A1}$$

where 2Δ is the superconducting gap, $\epsilon_{\mathbf{p}}$ is the single-particle energy of the electron measured with respect to the chemical potential μ, and $E_{\mathbf{p}} \equiv \sqrt{\epsilon_{\mathbf{p}}^2 + \Delta^2}$ is the quasiparticle excitation energy. The sum in (A1) can be converted into an integral, which can be evaluated analytically (see Sec. II for details). This gives us the real and imaginary parts (we will use $P_{k\omega}$ instead of $P_{\mathbf{k}\omega}$ in what follows):

$$P_{k\omega}^R = \frac{p_{SF}^2 k^2}{2\pi m_S}\frac{1}{\omega^2 - 4\Delta^2}, \quad P_{k\omega}^I = \begin{cases} 0, & 0 \leqslant \omega \leqslant 2\Delta \\ -\frac{p_{SF}^2 k^2}{2m_S\omega}\frac{1}{\sqrt{\omega^2 - 4\Delta^2}}, & 2\Delta < \omega \end{cases} \tag{A2}$$

where p_{SF} is the Fermi momentum and m_S is effective electron mass in the superconductor.

The calculation of the electron gas polarization is standard [35] and here we simply provide the result:

$$\Pi^R_{k\omega} = \frac{p_{NF}^2}{2\pi m_N}\frac{k^2}{\omega^2},$$

$$\Pi^I_{k\omega} = \begin{cases} -\frac{m_N}{\pi}\Big[\sqrt{1-\big(\frac{m_N\omega}{p_{NF}k}-\frac{k}{2p_{NF}}\big)^2}-\sqrt{1-\big(\frac{m_N\omega}{p_{NF}k}+\frac{k}{2p_{NF}}\big)^2}\Big], & 0\leqslant\omega<\frac{p_{NF}}{m_N}k-\frac{k^2}{2m_N} \\ -\frac{m_N}{\pi}\sqrt{1-\big(\frac{m_N\omega}{p_{NF}k}-\frac{k}{2p_{NF}}\big)^2}, & \frac{p_{NF}}{m_N}k-\frac{k^2}{2m_N}<\omega<\frac{p_{NF}}{m_N}k+\frac{k^2}{2m_N} \\ 0, & \frac{p_{NF}}{m_N}k+\frac{k^2}{2m_N}<\omega \end{cases} \tag{A3}$$

where p_{NF} and m_N are the Fermi momentum and electron effective mass in the normal metal layer, respectively.

Using the linear response theory, we can represent the electron density fluctuations in the normal layer $\delta n_{k\omega}$ and Cooper pair density fluctuations in superconducting layer $\delta N_{k\omega}$ as

$$\delta n_{k\omega} = \Pi_{k\omega}\big(v_k\delta n_{k\omega}+u_k\delta N_{k\omega}+W^{(N)}_{k\omega}\big),\quad \delta N_{k\omega} = P_{k\omega}\big(v_k\delta N_{k\omega}+u_k\delta n_{k\omega}+W^{(S)}_{k\omega}\big), \tag{A4}$$

where $W^{(N)}_{k\omega}$ and $W^{(S)}_{k\omega}$ are the Fourier images of the potential energy caused by the external electric field (see also Appendix C for details):

$$W^{(N)}_{k\omega} = g_N\frac{eE_0}{ik},\quad W^{(S)}_{k\omega} = g_S\frac{eE_0}{ik}, \tag{A5}$$

where the couplings $g_N = 0, 1$ and $g_S = 0, 1$ allow us to turn off the external field on either of the layers. In matrix form, Eq. (A4) reads as

$$\begin{bmatrix}\Pi_{k\omega}v_k-1 & \Pi_{k\omega}u_k\\ P_{k\omega}u_k & P_{k\omega}v_k-1\end{bmatrix}\begin{bmatrix}\delta n_{k\omega}\\ \delta N_{k\omega}\end{bmatrix} = -\begin{bmatrix}\Pi_{k\omega}W^{(N)}_{k\omega}\\ P_{k\omega}W^{(S)}_{k\omega}\end{bmatrix}. \tag{A6}$$

The eigenmodes of the system can then be found by equating the determinant of the 2×2 matrix in (A6) to zero, which yields

$$1-v_k(\Pi_{k\omega}+P_{k\omega})+\big(v_k^2-u_k^2\big)\Pi_{k\omega}P_{k\omega} = 0. \tag{A7}$$

In particular, for the real part of this determinant we have

$$D^R_{k\omega}\equiv 1-v_k\big(\Pi^R_{k\omega}+P^R_{k\omega}\big)+\big(v_k^2-u_k^2\big)\Pi^R_{k\omega}P^R_{k\omega}+\Pi^I_{k\omega}P^I_{k\omega}\big(u_k^2-v_k^2\big) = 0. \tag{A8}$$

Using Eqs. (A2) and (A3), we find that $\Pi^I_{k\omega} = 0$ for $\omega > 2\Delta$ while $P^I_{k\omega} = 0$ for $\omega < 2\Delta$. Hence, the last term in Eq. (A8) is zero for all positive ω and we have

$$1-v_k\big(\Pi^R_{k\omega}+P^R_{k\omega}\big)+\big(v_k^2-u_k^2\big)\Pi^R_{k\omega}P^R_{k\omega} = 0. \tag{A9}$$

Solving for ω, we find two branches of dispersion of the hybrid modes [see Fig. 1(b) in the main text]

$$\omega^2_\pm(k) = 2\Delta^2+e^2k\left(\frac{p_{NF}^2}{m_N}+\frac{p_{SF}^2}{m_S}\right)$$
$$\pm\frac{1}{2}\sqrt{\left[\left(2\Delta-ep_{NF}\sqrt{\frac{k}{m_N}}\right)^2+\frac{e^2}{m_S}p_{SF}^2k\right]\left[\left(2\Delta+ep_{NF}\sqrt{\frac{k}{m_N}}\right)^2+\frac{e^2}{m_S}p_{SF}^2k\right]-4\beta_k^2}, \tag{A10}$$

where $\beta_k^2\equiv\frac{e^4p_{NF}^2p_{SF}^2}{m_Nm_S}k^2(1-e^{-2ka})$.

When the interlayer interaction is turned off, by separating them sufficiently far apart, for example, the individual bare modes of the 2DEG and the superconductor have similar form as Eq. (A10) except that we replace the last term inside the square root by $\beta^2_{k,\mathrm{bare}}\equiv\frac{e^4p_{NF}^2p_{SF}^2}{m_Nm_S}k^2$.

1. EM power absorption by 2DEG

Further, the matrix equation (A6) can be solved for the density fluctuations which yields

$$\delta n_{k\omega} = \frac{eE_0}{k}\frac{\big(N^R_{k\omega}+iN^I_{k\omega}\big)D^R_{k\omega}+\big(N^I_{k\omega}-iN^R_{k\omega}\big)D^I_{k\omega}}{\big(D^R_{k\omega}\big)^2+\big(D^I_{k\omega}\big)^2}, \tag{A11}$$

where

$$\begin{aligned} N^R_{k\omega} &= (g_N u_k - g_S v_k)\big(\Pi^I_{k\omega} P^R_{k\omega} + \Pi^R_{k\omega} P^I_{k\omega}\big) + g_N \Pi^I_{k\omega}, \\ N^I_{k\omega} &= -(g_N u_k - g_S v_k)\Pi^R_{k\omega} P^R_{k\omega} - g_N \Pi^R_{k\omega}, \\ D^I_{k\omega} &= \big(v_k^2 - u_k^2\big)\big(P^I_{k\omega}\Pi^R_{k\omega} - P^R_{k\omega}\Pi^I_{k\omega}\big) - v_k\big(P^I_{k\omega} + \Pi^R_{k\omega}\big). \end{aligned} \tag{A12}$$

Here, $D^R_{k\omega}$ has already been given in Eq. (A8). We are interested in the real part of (A11) only, therefore, we restrict ourselves to

$$\delta n_{k\omega} = \frac{eE_0}{k}\frac{N^R_{k\omega}D^R_{k\omega} + N^I_{k\omega}D^I_{k\omega}}{\big(D^R_{k\omega}\big)^2 + (D^I_{k\omega})^2}. \tag{A13}$$

Further, under the assumption of linear response of the system, the Fourier component of the current in the 2DEG layer can be written as

$$J_{k'\omega'} = (2\pi)^3\delta^{(2)}(\mathbf{k}' - \mathbf{k}_\parallel)\delta(\omega' - \omega)j_{k'\omega}. \tag{A14}$$

The Dirac delta functions in (A14) explicitly implement the linear response assumption. Thus, both ω' and $\mathbf{k}'$ have specific values fixed by the external electromagnetic field [the factor $(2\pi)^3$ is written for notational aesthetics]. Since $\mathbf{E}(\mathbf{r},t)$ and $\mathbf{J}(\mathbf{r},t)$ have the same wave vector and frequency, the following formula can be used to compute the time-averaged power absorbed by the hybrid system as a function of frequency ω:

$$\mathcal{P}(\omega) = \frac{1}{2}\bigg\langle \mathrm{Re}\int d^2r\, \mathbf{J}(\mathbf{r},t)\cdot\mathbf{E}^*(\mathbf{r},t)\bigg\rangle, \tag{A15}$$

where the integration is over the plane of the normal metal sample and $\langle\ldots\rangle$ denotes time averaging. Normalizing Eq. (A15) by $\int d^2r = L^2$, we obtain the specific power absorption coefficient (later simply referred to as *power absorption*)

$$P_1(\omega) \equiv \frac{\mathcal{P}(\omega)}{L^2} = \frac{1}{2}\mathrm{Re}(j_{k\omega}E_0). \tag{A16}$$

Utilizing the continuity equation $kj_{k,\omega} = -e\omega\delta n_{k,\omega}$ together with Eq. (A13), we find

$$\begin{aligned} P_1(\omega) &= \frac{1}{2}\frac{e\omega}{k}\big|\mathrm{Re}(\delta n_{k,\omega})\big|E_0 \\ &= \frac{e^2\omega E_0^2}{2k^2}\left|\frac{N^R_{k\omega}D^R_{k\omega} + N^I_{k\omega}D^I_{k\omega}}{\big(D^R_{k\omega}\big)^2 + \big(D^I_{k\omega}\big)^2}\right|. \end{aligned} \tag{A17}$$

2. EM power absorption by superconductor

We can follow a similar procedure to calculate the current of Cooper pairs in the superconductor (see also Appendix B). The power absorption then reads as

$$\begin{aligned} P_2(\omega) &= \frac{1}{2}\frac{2e\omega}{k}|\mathrm{Re}(\delta N_{k\omega})|E_0 \\ &= \frac{e^2\omega E_0^2}{k^2}\left|\frac{M^R_{k\omega}D^R_{k\omega} + M^I_{k\omega}D^I_{k\omega}}{\big(D^R_{k\omega}\big)^2 + \big(D^I_{k\omega}\big)^2}\right|, \end{aligned} \tag{A18}$$

where

$$M^R_{k\omega} = (g_N u_k - g_S v_k)\big(P^R_{k\omega}\Pi^I_{k\omega} + P^I_{k\omega}\Pi^R_{k\omega}\big) + g_S P^I_{k\omega}, \quad M^I_{k\omega} = (g_S v_k - g_N u_k)P^R_{k\omega}\Pi^R_{k\omega} - g_S P^R_{k\omega}. \tag{A19}$$

APPENDIX B: EVALUATION OF POLARIZATION FUNCTIONS

We consider the retarded polarization operator of the superconductor at zero temperature. Its general form, up to one-loop order, is given by

$$P^{\mathrm{ret}}_{k\omega} = \sum_{\mathbf{p}}\frac{E_{\mathbf{p}}E_{\mathbf{p+k}} - \xi_{\mathbf{p}}\xi_{\mathbf{p+k}} - \Delta^*_{\mathbf{p}}\Delta_{\mathbf{p+k}}}{E_{\mathbf{p}}E_{\mathbf{p+k}}}\left(\frac{1}{\omega + i\delta - E_{\mathbf{p}} - E_{\mathbf{p+k}}} - \frac{1}{\omega + i\delta + E_{\mathbf{p}} + E_{\mathbf{p+k}}}\right). \tag{B1}$$

Let us evaluate the real $P^R_{k\omega}$ and imaginary $P^I_{k\omega}$ parts of this polarization operator ($P^{\mathrm{ret}}_{k\omega} = P^R_{k\omega} + iP^I_{k\omega}$) separately.

1. *S* wave, real part

In the case of s-wave pairing, the gap is independent of the momentum. The real part then reads as

$$P_{k\omega}^{R}=\sum_{\mathbf{p}}\frac{E_{\mathbf{p}}E_{\mathbf{p}+\mathbf{k}}-\xi_{\mathbf{p}}\xi_{\mathbf{p}+\mathbf{k}}-\Delta^2}{E_{\mathbf{p}}E_{\mathbf{p}+\mathbf{k}}}\left(\frac{1}{\omega-E_{\mathbf{p}}-E_{\mathbf{p}+\mathbf{k}}}-\frac{1}{\omega+E_{\mathbf{p}}+E_{\mathbf{p}+\mathbf{k}}}\right). \tag{B2}$$

First, we can convert the sum in Eq. (B2) into an integral by the replacement

$$\sum_{\mathbf{p}}\to\frac{1}{(2\pi)^2}\int d^2p=\frac{1}{(2\pi)^2}\int_0^{\infty}dp\,p\int_0^{2\pi}d\phi. \tag{B3}$$

Without loss of generality, we choose $\mathbf{k}$ to point along the positive x direction, so that ϕ is the angle between $\mathbf{p}$ and $\mathbf{k}$. We then perform the change of integration variable $\phi\to p_1$:

$$p_1^2\equiv|\mathbf{p}+\mathbf{k}|^2=p^2+2kp\cos\phi+k^2,\quad d\phi=-\frac{p_1dp_1}{pk\sin\phi}, \tag{B4}$$

where

$$\sin\phi=\pm\sqrt{1-\left(\frac{p_1^2-p^2-k^2}{2pk}\right)^2} \tag{B5}$$

with the positive sign for $\phi\in[0,\pi]$ and negative sign for $\phi\in[\pi,2\pi]$. The integration over ϕ in Eq. (B3) becomes

$$\int_0^{2\pi}d\phi=\int_0^{\pi}d\phi+\int_{\pi}^{2\pi}d\phi=4\int_{p-k}^{p+k}\frac{p_1dp_1}{\sqrt{\left[(p+k)^2-p_1^2\right]\left[p_1^2-(p-k)^2\right]}}. \tag{B6}$$

Next, we can change the integration variables further:

$$p\to\xi_p=\frac{p^2}{2m}-\mu,\quad dp=\sqrt{\frac{m}{2(\xi_p+\mu)}}d\xi_p. \tag{B7}$$

A similar change of variable is also done for $p_1\to\xi_1=\frac{p_1^2}{2m}-\mu$. Equation (B2) now turns into

$$P_{k\omega}^{R}=\frac{m^2}{\pi^2}\int_{-\infty}^{\infty}d\xi_p\int_{\xi_{p-k}}^{\xi_{p+k}}d\xi_1\frac{E_pE_1-\xi_p\xi_1-\Delta^2}{E_pE_1}\left(\frac{1}{\omega-E_p-E_1}-\frac{1}{\omega+E_p+E_1}\right)$$
$$\times\frac{1}{\sqrt{\{[\sqrt{2m(\xi_p+\mu)}+k]^2-2m(\xi_1+\mu)\}\{2m(\xi_1+\mu)-[\sqrt{2m(\xi_p+\mu)}-k]^2\}}}, \tag{B8}$$

where $E_p=\sqrt{\xi_p^2+\Delta^2}$ and $E_1=\sqrt{\xi_1^2+\Delta^2}$. We should point out some important nuances in the equation above. First, the lower bound of the integral over ξ_p is originally $-\mu$. This energy lies deep in the Fermi sea so that we can extend it to negative infinity without incurring significant error.

The factors inside the radical in the last line of Eq. (B8) can be simplified by using the fact that the significant contribution to the integral is from a small interval within the Fermi momentum p_F so that

$$\sqrt{\frac{2(\xi_p+\mu)}{m}}\approx v_F, \tag{B9}$$

and that we are interested in small wave vectors $k\approx 0$ so that terms of order k^2 can be neglected. These approximations give

$$(\sqrt{2m(\xi_p+\mu)}+k)^2-2m(\xi_p+\mu)\approx 2m(\xi_p-\xi_1+v_Fk),\quad 2m(\xi_p+\mu)-(\sqrt{2m(\xi_p+\mu)}+k)^2\approx 2m(\xi_1-\xi_p+v_Fk). \tag{B10}$$

Further, we change the integration variable $y\equiv\xi_1-\xi_p$ and simplify the factor

$$\frac{E_pE_1-\xi_p\xi_1-\Delta^2}{E_1}=\frac{\sqrt{\xi_p^2+\Delta^2}\sqrt{(\xi_p+y)^2+\Delta^2}-\xi_p(\xi_p+y)-\Delta^2}{\sqrt{(\xi_p+y)^2+\Delta^2}}. \tag{B11}$$

We are interested in the case when the wavelength is much longer than the size of the Cooper pairs, $v_Fk\ll\Delta$. Since $|y|<v_Fk$, we can expand Eq. (B11) in the vicinity of $y\approx 0$ and retain only the leading order. We have

$$\frac{E_pE_1-\xi_p\xi_1-\Delta^2}{E_1}\approx\frac{\Delta^2y^2}{2\left(\Delta^2+\xi_p^2\right)^{3/2}}. \tag{B12}$$

Collecting all these results, we find that Eq. (B8) turns into

$$P^R_{k\omega} = \frac{m\Delta^2}{4\pi^2}\int_{-\infty}^{\infty} d\xi_p \int_{-v_F k}^{v_F k} dy \frac{y^2}{\left(\xi_p^2+\Delta^2\right)^2}\frac{1}{\sqrt{(v_F k - y)(v_F k + y)}}$$
$$\times\left(\frac{1}{\omega-\sqrt{\xi_p^2+\Delta^2}-\sqrt{(\xi_p+y)^2+\Delta^2}}-\frac{1}{\omega+\sqrt{\xi_p^2+\Delta^2}+\sqrt{(\xi_p+y)^2+\Delta^2}}\right). \tag{B13}$$

Using the smallness of y, we can similarly expand the second line in Eq. (B13) as

$$\frac{1}{\omega\mp\sqrt{\xi_p^2+\Delta^2}\mp\sqrt{(\xi_p+y)^2+\Delta^2}} \approx \frac{1}{\omega\mp 2E_p}. \tag{B14}$$

Substitution of this expression into Eq. (B13) enables us to evaluate the integral over y by letting $x \equiv y/(v_F k)$:

$$\int_{-v_F k}^{v_F k} \frac{y^2 dy}{\sqrt{(v_F k - y)(v_F k + y)}} = (v_F k)^2 \int_{-1}^{1} \frac{x^2 dx}{\sqrt{(1-x)(1+x)}} = (v_F k)^2 \frac{\pi}{2}. \tag{B15}$$

Equation (B13) turns into

$$P^R_{k\omega} = \frac{m\Delta^2}{8\pi}(v_F k)^2 \int_{-\infty}^{\infty} d\xi_p \frac{1}{\left(\xi_p^2+\Delta^2\right)^2}\left(\frac{1}{\omega-2\sqrt{\xi_p^2+\Delta^2}}-\frac{1}{\omega+2\sqrt{\xi_p^2+\Delta^2}}\right)$$
$$= \frac{m\Delta^2}{8\pi}(v_F k)^2 \int_{-\infty}^{\infty} d\xi_p \frac{1}{\left(\xi_p^2+\Delta^2\right)^{3/2}}\frac{1}{\frac{1}{4}\omega^2-\Delta^2-\xi_p^2}. \tag{B16}$$

We denote $\alpha \equiv \sqrt{\frac{1}{4}\omega^2-\Delta^2}$ and then rewrite $P^R_{k\omega}$ as

$$P^R_{k\omega} = \frac{m(v_F k\Delta)^2}{8\pi}\int_{-\infty}^{\infty} d\xi_p \frac{1}{\left(\xi_p^2+\Delta^2\right)^{3/2}}\frac{1}{\alpha^2-\xi_p^2}. \tag{B17}$$

Note that the integrand in Eq. (B17) has vanishing contribution for large ξ_p. In the high-frequency regime $\omega \gg 2\sqrt{2}\Delta$, $\alpha > \Delta$ so that the integral has negligible contribution for $\xi_p > \alpha$. We can then expand

$$\frac{1}{\alpha^2-\xi_p^2} \approx \frac{1}{\alpha^2}. \tag{B18}$$

Putting $\xi_p = \Delta \sinh t$ in the integral in Eq. (B17), we find

$$\int_{-\infty}^{\infty} d\xi_p \frac{1}{\left(\xi_p^2+\Delta^2\right)^{3/2}} = \frac{1}{\Delta^2}\int_{-\infty}^{\infty} \operatorname{sech}^2 t\, dt = \frac{1}{\Delta^2}\tanh t\,|_{-\infty}^{\infty} = \frac{2}{\Delta^2}, \tag{B19}$$

and Eq. (B17) then turns into

$$P^R_{k\omega} = \frac{m v_F^2 k^2}{\pi}\frac{1}{\omega^2-4\Delta^2}, \qquad \omega \gg 2\sqrt{2}\Delta. \tag{B20}$$

2. *S* wave, imaginary part

A similar manipulation can be performed to evaluate the imaginary part of Eq. (B1):

$$iP^I_{k\omega} = \frac{1}{(2\pi)^2}\int d^2p \frac{E_{\mathbf{p}}E_{\mathbf{p+k}}-\xi_{\mathbf{p}}\xi_{\mathbf{p+k}}-\Delta^2}{E_{\mathbf{p}}E_{\mathbf{p+k}}}[-i\pi\delta(\omega-E_{\mathbf{p}}-E_{\mathbf{p+k}})+i\pi\delta(\omega+E_{\mathbf{p}}+E_{\mathbf{p+k}})]. \tag{B21}$$

Since $\omega + E_{\mathbf{p}} + E_{\mathbf{p+k}} > 0$, the second Dirac delta function gives zero. We then have

$$P^I_{k\omega} = -\frac{m}{2\pi}\int_{-v_F k}^{v_F k} dy \frac{1}{\sqrt{(v_F k - y)(v_F k + y)}}\int_{-\infty}^{+\infty}\frac{d\xi_{\mathbf{p}}}{2E_{\mathbf{p}}^2}\delta(\omega-E_{\mathbf{p}}-E_{\mathbf{q},y}), \tag{B22}$$

where $E_{\mathbf{q},y} \equiv \sqrt{(y+\sqrt{E_p^2-\Delta^2})^2+\Delta^2}$. Note that since $E_{\mathbf{p}}, E_{\mathbf{p+k}} \geqslant \Delta$, it follows that $P^I_{k\omega} = 0$ when $\omega < 2\Delta$. For $\omega \geqslant 2\Delta$, we have

$$P^I_{k\omega} = -\frac{m}{8}(v_F k)^2 \sum_n \int_{-\infty}^{\infty}\frac{d\xi_p}{E_p^2}\frac{\delta(\xi_p-\xi_n)}{|f'(\xi_n)|}, \tag{B23}$$

where $f(\xi_p) \equiv E_p + E_q - \omega$ and the prime means derivative with respect to ξ_p. The sum is over the zeros of $f(\xi_n) = 0$. Since $|y| < v_F k \ll \Delta$, it follows that $E_{q,y} \approx E_p$ which then gives the zeros of $f(\xi_p)$ which are $\xi_n = \pm\sqrt{\frac{1}{4}\omega^2 - \Delta^2}$. Finally, we find

$$P^I_{k\omega} = -\frac{m}{2}(v_F k)^2 \frac{1}{\sqrt{\omega^2 - 4\Delta^2}}. \tag{B24}$$

3. *P* wave, real part

For the p-wave pairing, we can write the gap function as

$$\Delta_{\mathbf{k}} = f(k)(k_x - ik_y) = f(k)ke^{-i\phi}, \tag{B25}$$

where ϕ is the polar angle measured with respect to the k_x axis in k space. The function $f(k)$ can be found for the concrete p-wave superconductor. Here, we keep its general form, which should satisfy the following requirements: (i) $f(k)$ is finite for all $k \in [0, \infty)$ and (ii) $f(k)$ vanishes as $k \to \infty$. In our case, we take $f(k)$ to be Gaussian:

$$f(k) = Ae^{-\alpha k^2}, \tag{B26}$$

where A and α are phenomenological parameters. It should be noted that finding the exact shape of $f(k)$ is unnecessary when we are after the topological properties of the p-wave superconductor only [as long as $f(k)$ satisfies the requirements stated above].

The real part of the polarization can now be written as

$$\begin{aligned} P^R_{k\omega} = \frac{1}{(2\pi)^2}\int d^2p\Bigg[&\left(1 - \frac{\xi_{\mathbf{p}}\xi_{\mathbf{p+k}}}{E_{\mathbf{p}}E_{\mathbf{p+k}}} - \frac{\mathrm{Re}\{\Delta^*_{\mathbf{p}}\Delta_{\mathbf{p+k}}\}}{E_{\mathbf{p}}E_{\mathbf{p+k}}}\right)\left(\frac{1}{\omega - E_{\mathbf{p}} - E_{\mathbf{p+k}}} - \frac{1}{\omega + E_{\mathbf{p}} + E_{\mathbf{p+k}}}\right) \\ &+ \pi\frac{\mathrm{Im}\{\Delta^*_{\mathbf{p}}\Delta_{\mathbf{p+k}}\}}{E_{\mathbf{p}}E_{\mathbf{p+k}}}(\delta(\omega + E_{\mathbf{p}} + E_{\mathbf{p+k}}) - \delta(\omega - E_{\mathbf{p}} - E_{\mathbf{p-k}}))\Bigg]. \end{aligned} \tag{B27}$$

At the quantum critical point $\mu = 0$, the argument of the Dirac delta function $\delta(\omega + E_{\mathbf{p}} + E_{\mathbf{p+k}})$ vanishes at $\mathbf{k} = 0$ and $\omega = 0$. Since we are not interested in this critical case for now, we take $\mu \neq 0$ for which $\omega + E_{\mathbf{p}} + E_{\mathbf{p+k}} > 0$ and the mentioned Dirac delta is dropped.

Furthermore, we evaluate analytically the term involving the other Dirac delta. First, we rewrite

$$\Delta_{\mathbf{p+k}} = f(|\mathbf{p}+\mathbf{k}|)|\mathbf{p}+\mathbf{k}|e^{-i\theta}. \tag{B28}$$

Without loss of generality, we can choose $\mathbf{k}$ to lie along the p_x axis. We then find

$$\theta = \sin^{-1}(p\sin\phi), \tag{B29}$$

where ϕ is the polar angle and it is simultaneously the angle between $\mathbf{k}$ and $\mathbf{p}$.

Following a similar procedure as for the s-wave case, we put $p_1 \equiv |\mathbf{p}+\mathbf{k}|$ so that the Dirac delta term in Eq. (B27) becomes

$$\begin{aligned} P'^R_{k\omega} &= -\frac{1}{4\pi}\int d^2p\frac{\mathrm{Im}\{\Delta^*_{\mathbf{p}}\Delta_{\mathbf{p+k}}\}}{E_{\mathbf{p}}E_{\mathbf{p+k}}}\delta(\omega - E_{\mathbf{p}} - E_{\mathbf{p-k}}) \\ &= -\frac{1}{2\pi}\int_0^\infty\int_{p-k}^{p+k} dp_1\frac{f(p)f(p_1)p_1^2}{kE_{\mathbf{p}}E_{\mathbf{p+k}}}\cos\theta\,\delta(\omega - E_{\mathbf{p}} - E_{\mathbf{p-k}}), \end{aligned} \tag{B30}$$

where

$$\theta = \sin^{-1}\left[\frac{1}{2p_1k}\sqrt{4p^2k^2 - \left(p_1^2 - p^2 - k^2\right)^2}\right]. \tag{B31}$$

Then, we perform another change of integration variables:

$$\xi_p = \frac{p^2}{2m} - \mu, \quad \xi_{p_1} = \frac{p_1^2}{2m} - \mu, \tag{B32}$$

so that Eq. (B30) now becomes

$$P'^R_{k\omega} = -\frac{m\sqrt{2m}}{2\pi kv_F}\int_{-\infty}^{\infty} d\xi_p\int_{\xi_{p-k}}^{\xi_{p+k}} d\xi_1\frac{\sqrt{\xi_1+\mu}}{E_pE_1}f(\xi_p)f(\xi_1)\cos\theta\,\delta(\omega - E_p - E_1), \tag{B33}$$

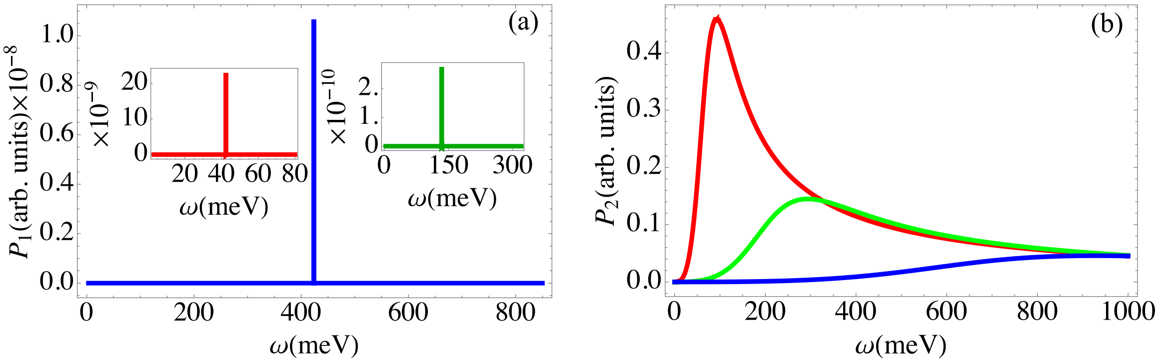

FIG. 4. Power absorption spectrum when the interlayer interaction is turned off. (a) Current is monitored in the 2DEG. (b) Current is monitored in the superconductor.

where $f(p) = A\exp\{-2m\alpha(\xi_p + \mu)\}$ and $E_p = \sqrt{\xi_p^2 + f^2(p)}$. The upper and lower limits of the ξ_1 integration can be rewritten as

$$\begin{aligned}\xi_{p\pm k} &= \frac{(p\pm k)^2}{2m} - \mu \\ &= \xi_p \pm v_F k + \frac{k^2}{2m}.\end{aligned} \tag{B34}$$

The relevant contribution from the ξ_p integration comes from a close neighborhood around the Fermi surface, so that ξ_p in Eq. (B9) we can approximate as $\xi_p \approx \frac{1}{2}mv_F^2 - \mu$. Further, since we are interested in small k, we can drop the k^2 term. The ξ_p and ξ_1 integrations in Eq. (B33) can now be interchanged and the former integral can be evaluated to get

$$P'^R_{k\omega} = -\frac{m\sqrt{2m}}{2\pi k v_F}\sum_{n=\pm}\int_{-v_F k}^{v_F k} d\xi_1 \frac{f(\xi_n)f(\xi_1)\sqrt{\xi_1+\mu}}{E_1|g'(\xi_n)|\sqrt{\xi_n^2+f_0^2}}\cos\theta, \tag{B35}$$

where $g(\xi_p) = E_p + E_1 - \omega$ and the prime over $g(\xi_p)$ denotes derivative with respect to ξ_p. The roots of $g(\xi_p) = 0$ are

$$\xi_\pm = -mf_0^2 \pm \frac{1}{2}\sqrt{4m^2 f_0^4 - 4\big[2m\mu f_0^2 - (\omega - E_1)^2\big]}. \tag{B36}$$

This last integral in (B35) can be easily evaluated numerically.

4. *P* wave, imaginary part

The imaginary part of the polarization operator reads as

$$\begin{aligned}P^I_{k\omega} = \frac{1}{(2\pi)^2}\int d^2p\bigg[\pi\bigg(1 - \frac{\xi_{\mathbf{p}}\xi_{\mathbf{p+k}}}{E_{\mathbf{p}}E_{\mathbf{p+k}}} - \frac{\mathrm{Re}\{\Delta^*_{\mathbf{p}}\Delta_{\mathbf{p+k}}\}}{E_{\mathbf{p}}E_{\mathbf{p+k}}}\bigg)(\delta(\omega + E_{\mathbf{p}} + E_{\mathbf{p+k}}) - \delta(\omega + E_{\mathbf{p}} - E_{\mathbf{p-k}})) \\ - \frac{\mathrm{Im}\{\Delta^*_{\mathbf{p}}\Delta_{\mathbf{p+k}}\}}{E_{\mathbf{p}}E_{\mathbf{p+k}}}\bigg(\frac{1}{\omega - E_{\mathbf{p}} - E_{\mathbf{p+k}}} - \frac{1}{\omega + E_{\mathbf{p}} + E_{\mathbf{p+k}}}\bigg)\bigg].\end{aligned} \tag{B37}$$

Similar steps (as in previous subsection) can be followed to find

$$\begin{aligned}P^I_{k\omega} = -\frac{m}{2\pi}\sum_{n=\pm}\int_{-v_F k}^{v_F k} d\xi_1 \frac{1}{|g'(\xi_n)|\sqrt{(\xi_n - \xi_1 + v_F k)(\xi_1 - \xi_n + v_F k)}} \\ \times\bigg(1 - \frac{\xi_n\xi_1}{E_n E_1} - \frac{\sqrt{m(\xi_1+\mu)}}{2\sqrt{2}kE_nE_1}f(\xi_n)f(\xi_1)[2m(\xi_1 - \xi_n) - k^2]\cos\theta\bigg).\end{aligned} \tag{B38}$$

APPENDIX C: EXTERNAL POTENTIAL $W_{k\omega}$

In terms of vector and scalar potentials, a time-dependent electric field is given by

$$\mathbf{E}(\mathbf{r},t) = -\frac{\partial\mathbf{A}}{\partial t} - \nabla\phi. \tag{C1}$$

Since the incident electric field is parallel to the plane of the electron gas sample at $z = 0$ and the tangential component of the electric field obeys the boundary condition $\lim_{z\to0^+} E_{||} = \lim_{z\to0^-} E_{||}$, we can neglect the effect of free charges on this field. Lorenz gauge then gives the wave equations

$$\nabla^2\phi - \frac{\partial^2\phi}{\partial t^2} = 0, \quad \nabla^2\mathbf{A} - \frac{\partial^2\mathbf{A}}{\partial t^2} = 0, \tag{C2}$$

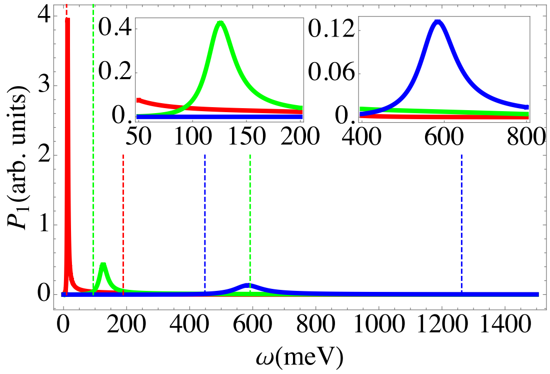

FIG. 5. Power absorption as a function of ω when there is no external EM field on the superconductor layer for $k = 1.0$ (red), 5.0×10^1 (green), 1.0×10^2 meV (blue). Inset: zoom-in for $50 \leqslant \omega < 200$ meV and $400 \leqslant \omega < 800$.

where ∇^2 is the Laplacian in three-dimensional space $\mathbf{R}$. It can be verified that

$$\phi(\mathbf{R}, t) = -x E_0 e^{-i(qz+\omega t)}, \tag{C3}$$

$$\mathbf{A}(\mathbf{R}, t) = \frac{qx}{\omega} E_0 e^{-i(qz+\omega t)} \hat{\mathbf{k}} \tag{C4}$$

obey the wave equations (C2) with $\omega = q$.

Note that Eq. (C3) is similar to the electrostatic case with uniform electric field along the x axis apart from the plane-wave factor. Hence, we can still use $W_{k\omega} = \frac{eE_0}{ik}$ analogous to the electrostatic case.

APPENDIX D: PHOTOABSORPTION SPECTRUM IN CASE IF THE INTERLAYER COUPLING IS SWITCHED OFF

Figure 4 shows the power spectrum when the coupling between the layers is switched off. The left-hand-side panel shows the case when the current is monitored in the 2DEG layer. It reveals a sharp peak contribution from the lower modes. This is expected since when there is no interlayer coupling, we have $P_1(\omega) \propto \Pi^I_{k\omega} = 0$ for $\omega > 2\Delta$. The sharp peaks occur at the lower hybrid modes where the denominator in the formula for $P_1(\omega)$ gives zero. Note the disappearance of three rightmost peaks (compare with Fig. 2 in the main text). This confirms that the three broad rightmost peaks in Fig. 2(b) are primarily due to the superconductor.

The right-hand-side panel similarly shows the case when the current is monitored in the superconductor layer. It shows that the three leftmost peaks disappear, which confirms that they are primarily due to the 2DEG layer.

APPENDIX E: EMF IS EXPOSED TO THE 2DEG ONLY

We now investigate the power absorption in the normal layer when the external EM field in the superconductor is

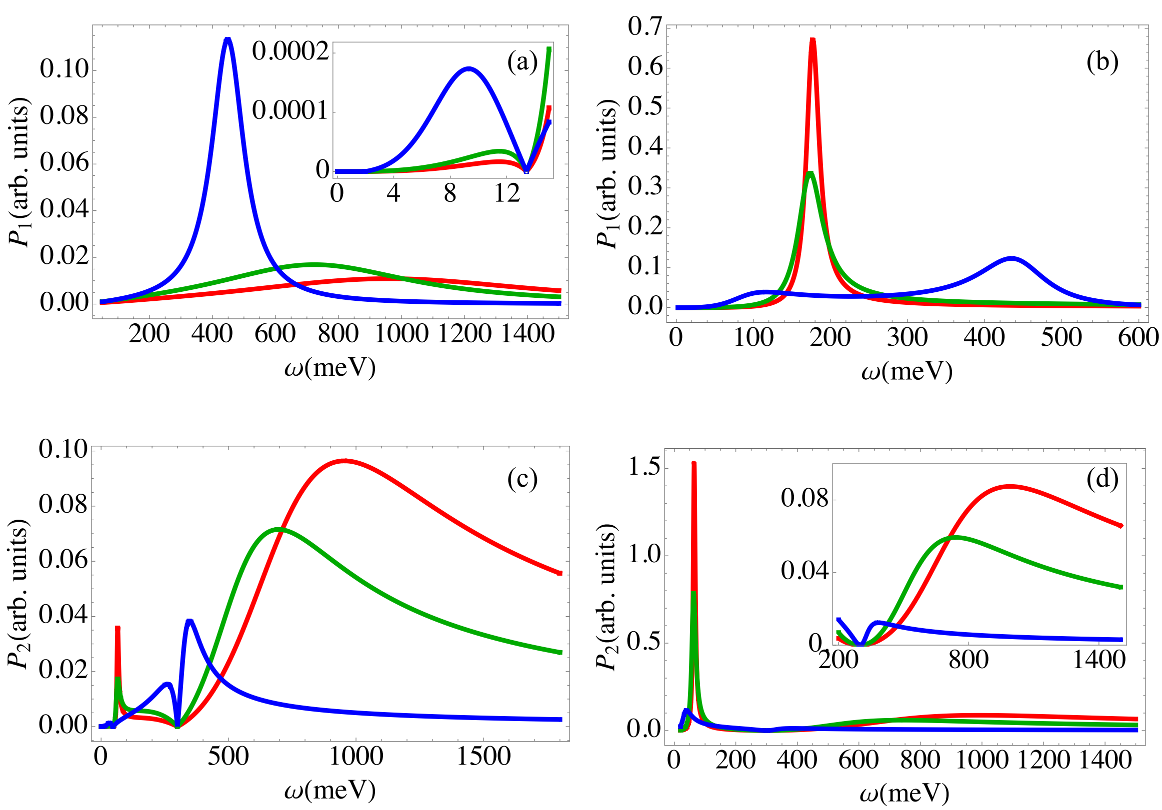

FIG. 6. Power absorption for $m_N = m_e$ and the effective electron mass in superconducting layer varied: $m_S = 0.5m_e$ (red), $m_S = m_e$ (green), $m_S = 10m_e$ (blue). Upper panels: current is monitored in the 2DEG with EM field present in (a) both layers and (b) 2DEG layer only. Lower two panels: current is monitored in the superconductor with EM field present in (c) both layers and (d) 2DEG layer only. Zoom-in for $0 \leqslant \omega < 14$ meV and $200 \leqslant \omega < 1500$.

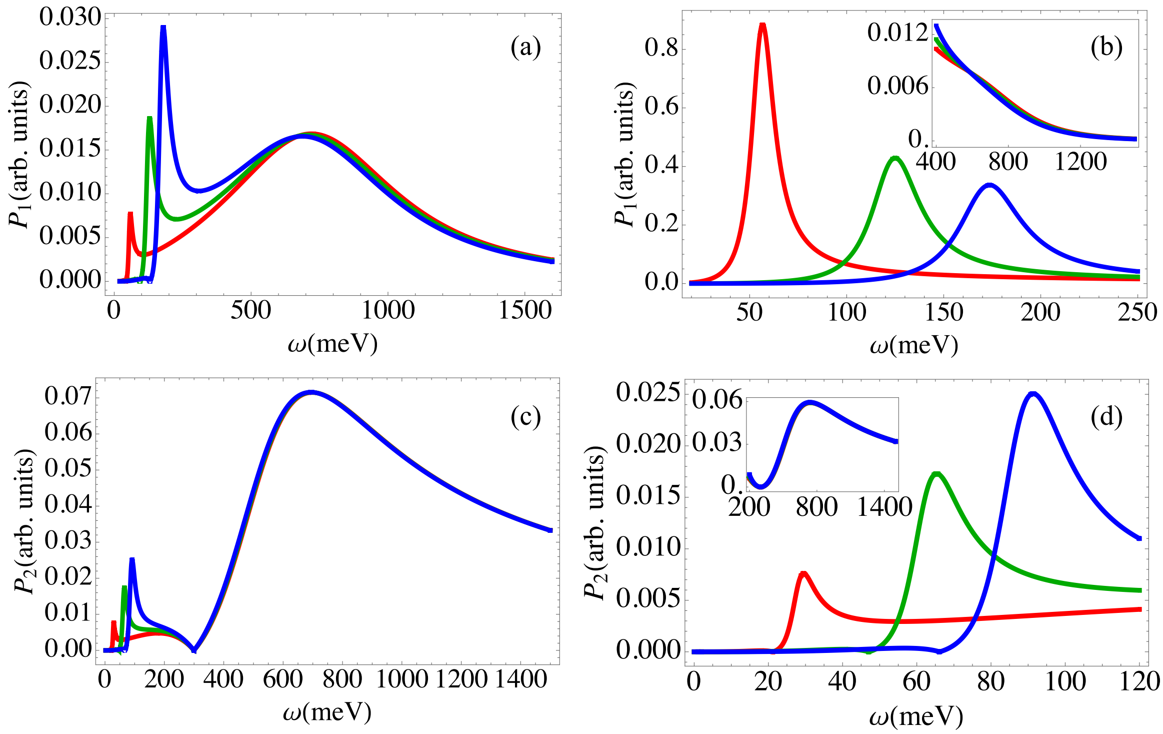

FIG. 7. Power absorption in the case when the interlayer spacing is varied (in eV^{-1}): 1.0×10^{-2} (red), 5.0×10^{-2} (green), and 1.0×10^{-1} (blue). Upper panels: current monitored in the 2DEG with EM field present in (a) both layers and (b) 2DEG layer only. Lower panels: current is monitored in the superconductor with EM field present in (c) both layers and (d) 2DEG layer only.

turned off by setting $g_N = 1$ and $g_S = 0$ in Eq. (A12) (see Fig. 5). It shows that the contribution of the upper hybrid modes decreases as compared to Fig. 2 in the main text and the curves in the vicinity of the upper hybrid modes are quite broad. The opposite is true for the lower hybrid modes: their contribution is significantly enhanced, as expected, since the superconductor is not exposed to light.

APPENDIX F: DEPENDENCE OF POWER ABSORPTION ON ELECTRON EFFECTIVE MASSES IN THE SUPERCONDUCTOR (m_S)

Figure 6 shows the power absorption when the effective mass of the electron in the superconductor layer m_S is varied. In general, the peak due to the upper hybrid mode becomes narrower when the mass m_S increases. When the current is monitored in the 2DEG, this peak increases, as can be seen in Fig. 6(a) while it decreases when the current is monitored in the superconductor layer [Figs. 6(c) and 6(d)]. The peak due to the lower hybrid mode in turn follows an opposite pattern: it decreases and becomes broader as m_S is increased, except when the current is monitored in 2DEG layer [Fig. 6(a), inset].

APPENDIX G: DEPENDENCE OF PHOTOABSORPTION ON THE INTERLAYER SPACING (a)

Figure 7 shows the power absorption when the layer spacing is varied. There is minimal effect on the peaks corresponding to the upper hybrid modes. In general, the peaks due to the lower hybrid modes increase with the layer spacing except in Fig. 7(b).

[1] C. L. Kane and E. J. Mele, Phys. Rev. Lett. **95**, 146802 (2005).
[2] C. L. Kane and E. J. Mele, Phys. Rev. Lett. **95**, 226801 (2005).
[3] B. A. Bernevig and S. C. Zhang, Phys. Rev. Lett. **96**, 106802 (2006).
[4] L. Fu and C. L. Kane, Phys. Rev. B **76**, 045302 (2007).
[5] F. V. Kusmartsev and A. M. Tsvelik, JETP Lett. **42**, 257 (1985).
[6] D. T. Son and B. Z. Spivak, Phys. Rev. B **88**, 104412 (2013).
[7] B. Q. Lv, H. M. Weng, B. B. Fu, X. P. Wang, H. Miao, J. Ma, P. Richard, X. C. Huang, L. X. Zhao, G. F. Chen, Z. Fang, X. Dai, T. Qian, and H. Ding, Phys. Rev. X **5**, 031013 (2015).
[8] A. A. Soluyanov, D. Gresch, Z. Wang, Q. Wu, M. Troyer, X. Dai, and B. A. Bernevig, Nature (London) **527**, 495 (2015).
[9] L. Yang, Z. Liu, Y. Sun, H. Peng, H. Yang, T. Zhang, B. Zhou, Y. Zhang, Y. Guo, and M. Rahn, Nat. Phys. **11**, 728 (2015).
[10] S.-Y. Xu, N. Alidoust, I. Belopolski, Z. Yuan, G. Bian, T.-R. Chang, H. Zheng, V. N. Strocov, D. S. Sanchez, G. Chang, C. Zhang, D. Mou, Y. Wu, L. Huang, C.-C. Lee, S.-M. Huang, B. K. Wang, A. Bansil, H.-T. Jeng, T. Neupert *et al.*, Nat. Phys. **11**, 748 (2015).
[11] C.-K. Chiu, J. C. Teo, A. P. Schnyder, and S. Ryu, Rev. Mod. Phys. **88**, 035005 (2016).

[12] Y. Sun, S. C. Wu, M. N. Ali, C. Felser, and B. Yan, Phys. Rev. B **92**, 161107 (2015).
[13] C.-L. Zhang, S. Y. Xu, I. Belopolski, Z. Yuan, Z. Lin, B. Tong, G. Bian, N. Alidoust, C. C. Lee, S. M. Huang, T-R. Chang, G. Chang, C.-H. Hsu, H.-T. Jeng, M. Neupane, D. S. Sanchez, H. Zheng, J. Wang, H. Lin, C. Zhang *et al.*, Nat. Commun. **7**, 10735 (2016).
[14] T. Van Duzer and S. Kumar, Cryogenics **30**, 1014 (1990).
[15] V. Mourik, K. Zuo, S. M. Frolov, S. R. Plissard, E. P. A. M. Bakkers, and L. P. Kouwenhoven, Science **336**, 1003 (2012).
[16] S. Takei, B. M. Fregoso, V. Galitski, and S. Das Sarma, Phys. Rev. B **87**, 014504 (2013).
[17] S. Takei and V. Galitski, Phys. Rev. B **86**, 054521 (2012).
[18] H. J. Suominen, M. Kjaergaard, A. R. Hamilton, J. Shabani, C. J. Palmstrom, C. M. Marcus, and F. Nichele, Phys. Rev. Lett. **119**, 176805 (2017).
[19] M. Khoshnegar and A. H. Majedi, Phys. Rev. B **84**, 104504 (2011).
[20] T. Wenger, G. Viola, J. Kinaret, M. Fogelström, and P. Tassin, 2D Mater. **4**, 025103 (2017).
[21] T. Wenger, G. Viola, J. Kinaret, M. Fogelström, and P. Tassin, Phys. Rev. B **97**, 085419 (2018).
[22] G. Viola, T. Wenger, J. Kinaret, and M. Fogelström, New J. Phys. **19**, 073027 (2017).
[23] G. Viola, T. Wenger, J. Kinaret, and M. Fogelström, Phys. Rev. B **97**, 085429 (2018).
[24] T. Wenger, G. Viola, M. Fogelström, P. Tassin, and J. Kinaret, Phys. Rev. B **94**, 205419 (2016).
[25] P. Skopelitis, E. D. Cherotchenko, A. V. Kavokin, and A. Posazhennikova, Phys. Rev. Lett. **120**, 107001 (2018).
[26] F. P. Laussy, A. V. Kavokin, and I. A. Shelykh, Phys. Rev. Lett. **104**, 106402 (2010).
[27] O. Cotlet, S. Zeytinoglu, M. Sigrist, E. Demler, and A. Imamoglu, Phys. Rev. B **93**, 054510 (2016).
[28] A. Hayat, P. Zareapour, Shu Yang F. Zhao, A. Jain, I. G. Savelyev, M. Blumin, Z. Xu, A. Yang, G. D. Gu, H. E. Ruda, S. Jia, R. J. Cava, A. M. Steinberg, and K. S. Burch, Phys. Rev. X **2**, 041019 (2012).
[29] J. Shabani, M. Kjaergaard, H. J. Suominen, Y. Kim, F. Nichele, K. Pakrouski, T. Stankevic, R. M. Lutchyn, P. Krogstrup, R. Feidenhans'l, S. Kraemer, C. Nayak, M. Troyer, C. M. Marcus, and C. J. Palmstrom, Phys. Rev. B **93**, 155402 (2016).
[30] J. M. Shainline, S. M. Buckley, R. P. Mirin, and S. W. Nam, Phys. Rev. Appl. **7**, 034013 (2017).
[31] R. Yan, G. Khalsa, S. Vishwanath, Y. Han, J. Wright, S. Rouvimov, D. Scott Katzer, N. Nepal, B. P. Downey, D. A. Muller, H. G. Xing, D. J. Meyer, and D. Jena, Nature (London) **555**, 183 (2018).
[32] A. E. Miroshnichenko, S. Flach, and Yu. S. Kivshar, Rev. Mod. Phys. **82**, 2257 (2010).
[33] M. V. Boev, V. M. Kovalev, and I. G. Savenko, Phys. Rev. B **94**, 241408(R) (2016).
[34] P. I. Arseev, S. O. Loiko, and N. K. Fedorov, Phys. Usp. **49**, 1 (2006).
[35] A. L. Fetter and J. D. Walecka, *Quantum Theory of Many-Particle Systems* (Dover, New York, 2003).
[36] K. T. Law, Patrick A. Lee, and T. K. Ng, Phys. Rev. Lett. **103**, 237001 (2009).
[37] A. Das, Y. Ronen, Y. Most, Y. Oreg, M. Heiblum, and H. Shtrikman, Nat. Phys. **8**, 887 (2012).
[38] A. D. K. Finck, D. J. Van Harlingen, P. K. Mohseni, K. Jung, and X. Li, Phys. Rev. Lett. **110**, 126406 (2013).
[39] E. J. H. Lee, X. Jiang, R. Aguado, G. Katsaros, C. M. Lieber, and S. De Franceschi, Phys. Rev. Lett. **109**, 186802 (2012).
[40] S. Cho, R. Zhong, J. A. Schneeloch, G. Gu, and N. Mason, Sci. Rep. **6**, 21767 (2016).
[41] H.-J. Chen, X.-W. Fang, C.-Z. Chen, Y. Li, and X.-D. Tang, Sci. Rep. **6**, 36600 (2016).
[42] M. Mitrano, A. Cantaluppi, D. Nicoletti, S. Kaiser, A. Perucchi, S. Lupi, P. Di Pietro, D. Pontiroli, M. Ricco, S. R. Clark, D. Jaksch, and A. Cavalleri, Nature (London) **530**, 461 (2016).